ARMA/NARMS 04-505

Why sand fails after water breakthrough

Gang Han
Terralog Technologies Inc, Calgary, AB, Canada

Maurice B. Dusseault
Porous Media Research Institute, University of Waterloo, Waterloo, ON, Canada

John Cook
Schlumberger Cambridge Research, Cambridge, England

This paper was prepared for presentation at Gulf Rocks 2004, the 6th North America Rock Mechanics Symposium (NARMS): Rock Mechanics Across Borders and Disciplines, held in Houston, Texas, June 5 – 9, 2004.

ABSTRACT: Based on research and model development, including a new rock strength model that considers the effects of both chemical reactions and capillarity changes, a new pressure model that calculates fluid pressure variations with water saturation, an improved nonlinearity model for rock deformation modulus, and a coupled analytical elastoplastic model for stress estimation, the mechanisms for sand instability have been identified, quantified, and compared to address the question of why sand often fails after water breakthrough in an oil well.

Model calculations indicate that, with increase of water saturation, sands tend to become weaker (strength reduction) and softer (stiffness reduction) while the loading stresses are elevated and the maximum shear stress moves outward into the reservoir (i.e. a larger zone is affected). For the case discussed, losses of both rock strength and modulus can be up to 80%, while the shear stresses can double because of fluid relative permeability changes and strength loss. Furthermore, after shear failure the sands are more easily detached from the rock matrix because of a decrease in tensile capillary strength with an increase of water saturation. Since the capillary strength is shown to depend only on water saturation, the sanding rate for each value of saturation is constant until destabilizing forces are changed, which leads to so-called episodic sand production after an oil well starts to produce water. These analytical tools can serve as a basis to develop more useful sand stability tools for multiphase fluid flow environments.

1. INTRODUCTION

It is estimated that, on average, companies produce three barrels of water for each barrel of oil [1], seventy percent of which comes from weakly consolidated or unconsolidated sandstone. The intrusion of formation water into water-wetted but oil-saturated sand, which is the usual case in oil fields, may trigger or worsen the sand instability that has been frequently observed both in the field [2, 3] and in the laboratory [4-6]. Some characteristics of water-related sand production are:

- Sands become unstable and start to flow after water intrusion even though no preceding sand production was observed [3,4], and massive sand production occurs when S_w reaches a particular value [6];
- For sanding wells, the average sanding rate during water breakthrough is higher than before breakthrough [2];
- The critical global pressure gradient that activates sanding drops when S_w increases [5]; and,
- Sanding appears as an episodic phenomenon: at a given S_w, a sand cavity starts to grow and then becomes stabilized; additional cavity growth episodes require either an increase of pressure gradient or a change in the water saturation value [5,6].

Extensive experiments have been carried out to study the effect of changes in S_w (or moisture content, humidity, etc.) on different rock samples, such as shale [7, 8], chalk [9-11], and sandstone [2, 5, 12-15]. The various possible mechanisms may be generalized as follows [16]:

- Chemical reactions between water and solids and the dissolution of cementitious materials may weaken the rock;
- Changes in the surface tension and capillary force may lower the cohesive strength;

- A higher pressure gradient may develop since the relative permeability of oil is decreased with an increase in S_w; therefore there is a higher fluid velocity and drag force (seepage force) that may destabilize the sand; and,
- Particles plucked out of the rock skeleton by fluid flow and the swelling of clay materials may block pore throats and locally increase the pressure gradient and thus increase the destabilizing force.

Although the influence of water influx and S_w on sand stability has been appreciated for several decades, quantitative models have proven difficult, as compared to single-phase frictional sand production models without capillarity. In this paper, a comprehensive study of why sand fails after water breakthrough is carried out. This is based on experimental findings and a series of mathematical models, including a rock strength model that considers strength weakening due to both the effects of chemical reactions and capillarity changes, a fluid pressure model based on micromechanics of a biphasic fluid environment, a coupled analytical elastoplastic model for stress estimation, and an improved nonlinear model for rock deformation modulus.

This article is one of a series of studies, and it focuses more on model results to reveal the physics involved in water-related sand production. More details of the developed models can be found in other publications [17-20].

2. MODEL DEVELOPMENT

2.1. Strength model

Although there may be several physical and chemical processes involved [16], the general trend is that an increase in water saturation reduces rock strength, to the extent of 8% [12] to 98% [13], depending on rock texture, mineralogy, fluid chemistry, time, etc.

While some still doubt the significance of capillary effect on rock stability [21], most believe that capillarity plays an important role in sand production after water breakthrough into an oil well [3,6,9]. Consider two identical particles contacting tangentially (Fig. 1); the capillary force (F_c) in the liquid menisci between particles can be expressed as (a Nomenclature follows the article)

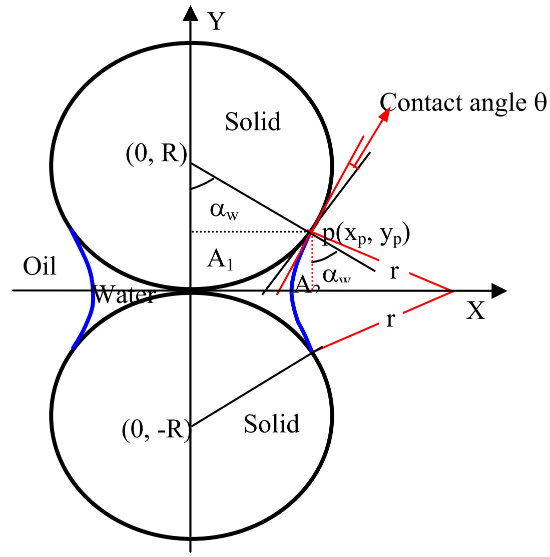

Fig. 1. Model for capillarity calculations

$$F_c = \pi x_p^{\;2} \Delta P \tag{1}$$

Assuming the shape of the liquid bridge is a toroid, the capillary pressure (ΔP) is

$$\Delta P = \gamma\left(\frac{1}{x_p} - \frac{1}{r}\right) \tag{2}$$

Using a Mohr-Coulomb (M-C) strength criterion, the unconfined compressive strength (σ_{UCS}) can be approximated as

$$\sigma_{UCS} = 2\frac{1-\phi}{\phi}\frac{\sin\varphi}{1-\sin\varphi}\frac{F_c}{R^2} \tag{3}$$

where φ is the graphical M-C friction angle, ϕ is rock porosity, and R is the radius of the spheres. Thus, the rock strength is related to rock porosity, friction angle, particle size and capillary force. Notice that in the equation the only variable changing with water saturation is F_c. With an assumption of zero contact angle, the water saturation S_w can be related to the geometrical parameters through [18]

$$\eta\phi S_w = -\frac{\alpha_w}{2} + \frac{1}{2}\tan\alpha_w + \left(\frac{\alpha_w}{2} - \frac{\pi}{4}\right)\left(\frac{1-\cos\alpha_w}{\cos\alpha_w}\right)^2 \tag{4}$$

where η is a factor accounting for non-uniform particle size effects on total rock strength [22].

Chemical reactions, such as quartz hydrolysis reducing silica-to-hydrogen bond energy, carbonate cement dissolution that physically changes the shape and size of cementitious deposits, new ferruginous mineral deposition, clay swelling, etc. are too difficult to be rigorously quantified with respect to sand stability [16]. An empirical approach using a time-exponential relationship is recommended for incorporating chemically reduced strength (C_{o_ch}) into stress calculations

$$C_{o\_ch} = a\exp(-bt) \tag{5}$$

where a and b are coefficients determined through curve fitting and t is time.

2.2. A pressure model at the microscopic level

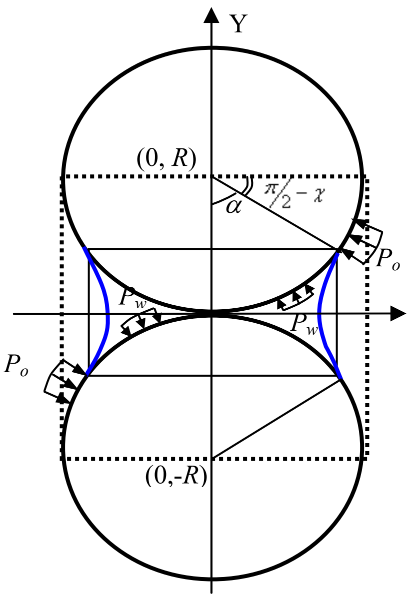

Fig. 2. Sketch of pore pressure calculations.

From Fig. 2, the force from the pore fluid pressure acting on the particle surface is

$$P(r)A = P_w(r)A_w + P_o(r)A_o \tag{6}$$

where subscripts w, o represent water phase and oil phase, respectively, P is an apparent fluid pressure at distance "r" from the wellbore and for use in the effective stress equations derived later, and A is the particle surface. The ratio of A_w/A and A_o/A can be derived within the dashed frame of Fig. 2 as

$$A_w/A = 2\alpha/\pi, \qquad A_o/A = 1 - 2\alpha/\pi \tag{7}$$

The difference of the two fluid pressures (P_w and P_o) is equal to the capillary pressure:

$$P_w - P_o = -P_c \tag{8}$$

Therefore, Eq. (6) becomes

$$P(r) = P_w(r) + P_c(1 - \frac{2\alpha}{\pi}) \tag{9}$$

or $$P(r) = P_o(r) - P_c\frac{2\alpha}{\pi} \tag{10}$$

Assuming steady-state fluid flow in an infinite reservoir, oil and water pressures are

$$P_w(r) = P_2 - \frac{Q_w\mu_w}{2\pi k k_{rw} h}\ln\left(\frac{R_2}{r}\right) \tag{11}$$

$$P_o(r) = P_2 - \frac{Q_o\mu_o}{2\pi k k_{ro} h}\ln\left(\frac{R_2}{r}\right) \tag{12}$$

where P_2 is far-field flowing pressure at distance R_2, h is reservoir thickness, k is absolute permeability; k_r is fluid relative permeability, Q is the fluid flow rate assumed, and μ is fluid viscosity. Substituting the pressures into Eq. (9), with constant total production rate ($Q = Q_w + Q_o$), an expression for pore pressure can be written as

$$P(r) = P_2 - \frac{Q\xi(S_w)}{2\pi k h}\ln\left(\frac{R_2}{r}\right) \tag{13}$$

where $$\xi(S_w) = \frac{2\alpha}{\pi}\frac{f_w}{k_{rw}/\mu_w} + \left(1 - \frac{2\alpha}{\pi}\right)\frac{f_o}{k_{ro}/\mu_o}.$$

Furthermore, f_w and f_o, water and oil fractions in fluid production respectively, can be related to each other through f_w = 1- f_o. The water fraction is then calculated through

$$f_w = \frac{Q_w}{Q} = \frac{-\frac{Akk_{rw}}{\mu_w}\frac{dP_w}{dr}}{-Ak(\frac{k_{rw}}{\mu_w}\frac{dP_w}{dr} + \frac{k_{ro}}{\mu_o}\frac{dP_o}{dr})} \tag{14}$$

Considering capillary pressure to be only related to water saturation (i.e. $dP_c/dr = 0$), the above equation becomes

$$f_w = \frac{1}{1 + \frac{k_{ro}\mu_w}{k_{rw}\mu_o}} \tag{15}$$

Since the value of the water volume angle α is related to water saturation through Eq. (4), there will be a specific value of pore pressure $P(r)$ associated with each value of water saturation.

2.3. Coupled elastoplastic model

For an elastic isotropic formation with a Biot coefficient of 1, stress equilibrium around a wellbore in a one-dimensional cylindrical system can be expressed as

$$\frac{\partial \sigma'_r}{\partial r} + \frac{\sigma'_r - \sigma'_\theta}{r} = \frac{\partial P}{\partial r} \tag{16}$$

Also, the stresses within the plastic zone must fulfill the M-C failure criterion

$$\sigma'_\theta = 2C_o \tan\beta + \sigma'_r \tan^2\beta \tag{17}$$

Because capillary strength resulting from fluid menisci mainly prevents particle separation rather than rotation, it acts more as a part of the cohesive M-C strength component. Thus, the cohesive shear strength C_o can be expressed as

$$C_o(S_w) = C_{o\_init} - C_{o\_ch} - \sigma_{UCS}(S_w)\tan\varphi \tag{18}$$

where C_{o_init} is the initial cohesive shear strength (before water breakthrough), and C_{o_ch} and σ_{UCS} are the reduced strengths that arise because of chemical reactions and capillarity.

The somewhat lengthy stress solutions can be found in a previous publication [19].

2.4. Nonlinearity modulus model

Besides effects on rock strength, water saturation changes can also lead to significant changes in the elastic properties. Young's modulus generally decreases with increase in water saturation [22-24], mimicking strength behavior in water-oil fluid environments, whereas Poisson's ratio may monotonously increase with saturation [12, 24] or remain constant [9], depending on rock type, mineralogy, and heterogeneity. In this research Poisson's ratio is assumed to remain constant.

Various nonlinear approaches have been developed to address stress-related nonlinear behavior in rock properties. They can be generalized into two categories: one is the nonlinearity due to shear damage caused by elevated shear stress [25, 26]

$$E = A_E\left(1 - \frac{R_f(1-\sin\varphi)(\sigma'_1 - \sigma'_3)}{2C_o\cos\varphi + 2\sigma'_3\sin\varphi}\right)^2 \tag{19}$$

where R_f is a parameter accounting for the effect of residual strength after the stress reaches a peak value, and A_E is the Young's modulus at initial stress state. The other category is the nonlinearity due to the confining stress compaction effect [27]:

$$E_i = E_a\left(1 + m_E \sigma_3'^{\,n_E}\right) \tag{20}$$

where E_a is the rock Young's modulus at atmospheric pressure, and m_E and n_E are constants determined from curve fitting. This equation was shown to be reasonable through a series of experiments [28]; therefore it is used in this study to calculate A_E in Eq. (19).

3. CALCULATIONS AND DISCUSSIONS

Besides the assumptions made with respect to the microscopic capillarity model [16], it is necessary to clearly restate some other model simplifications and assumptions before any further discussion:

- Rock particles are represented by spheres;
- No residual water or oil saturation is considered in the capillarity model;
- Biphasic fluid flow is steady, and capillary pressure around the wellbore is related only to water saturation;
- Stresses are calculated around an axisymmetric vertical wellbore in a one-dimensional cylindrical system in an isotropic formation with Biot coefficient of 1;
- Rock behaves elastoplastically and strength in the plastic zone is a constant for stress calculations; and,
- Rock stress-strain curves fit a hyperbolic relation in the nonlinearity modulus model.

Whereas these may be viewed as limitations to the models' applicability, the authors believe that because the models capture the essential physics, adjustments and calibrations can be incorporated to allow useful applications in real situations.

3.1. Strength weakening

With particle radius of 0.1 mm and surface tension of 0.036 N/m, the maximum capillary strength can be as high as 20 kPa (Fig. 3), whereas all capillary variables become zero around a saturation value of 0.34. The magnitude of the capillary strength is closely related to particle radius, surface tension, liquid-solid contact angle, size difference and the distance between particles, and the irregularity of particle surfaces [18]. However, there is a small section of the relationship at a water saturation approaching zero where a short rapid increase of strength is predicted because some volume of water is needed to build a stable liquid bridge between particles. This has been confirmed by an experiment in which a stable arch is found to develop with a small increase in water saturation in

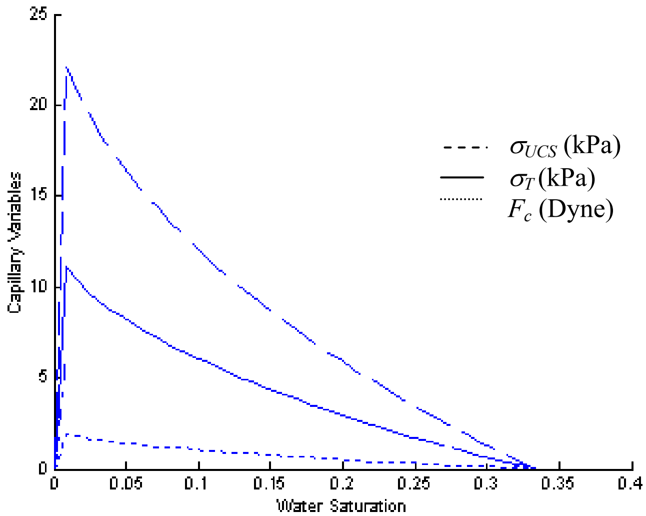

Fig. 3. Capillary force and strengths vs. water saturation.

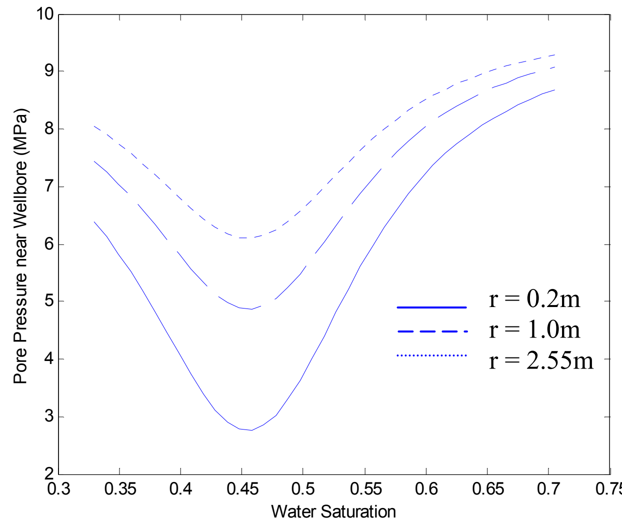

Fig. 4. Pore pressure at different locations with saturation

a biphasic fluid environment, whereas such an arch cannot be stable in a single-phase condition [6].

3.2. *Fluid pressure fluctuations*

For pressure and stress calculations, the water saturation in the microscopic model developed above should be calibrated to experimentally determined values. The saturation discrepancy between the model and reality results mainly from two sources that the microscopic model cannot address: one is connate water saturation (S_{wc}) and immobile oil saturation (S_{oi}); the other is the wettability effect for irregular particle surfaces. Assuming water saturation remains as a constant (S_{wc}) until water breakthrough occurs, the calibration can be carried out as

$$S'_w = S_{wc} + S_w * (1 - S_{wc} - S_{oi}) / S_{w0} \quad (21)$$

where S_{w0} is the saturation at which capillary pressure becomes zero.

Table 1. Relative permeabilities vs. saturation

S_w	k_{rw}	k_{row}
0.32	0	1
0.375	0.003	0.653
0.415	0.008	0.436
0.4555	0.017	0.311
0.495	0.028	0.214
0.535	0.057	0.14
0.575	0.091	0.089
0.615	0.134	0.049
0.655	0.184	0.019
0.694	0.242	0.001
0.734	0.301	0

Using the relative permeability data in Table 1, calculations of pressure redistributions with water saturation at different distance (r = 0.2 m, 1.0 m, 2.55 m) from the wellbore are plotted in Fig. 4. Interestingly, pore pressure first decreases with saturation until some critical saturation is reached (S_w = 0.45), and the decrease in magnitude can be as high as several MPa; then, it increases continuously to a value (when S_w = 0.734) even higher than initially (when S_w = 0.32). Furthermore, the pressure decrease becomes more significant closer to the wellbore, as illustrated by solid line in Fig. 4 (i.e. r = 0.2m). Physically, because water is a less viscous and more mobile fluid than oil, less energy is needed to drive it into the wellbore; consequently, the increase of water relative permeability raises the pore pressure whereas increase in oil relative permeability lowers it. The synthesis of both effects indicates that pore pressure in a water-dominant fluid system is relatively higher than in an oil-dominant fluid system.

The precision of pressure solutions from the new approach based on grain-scale physics is in the order of 10^{-15} comparing to the conventional method ($P = P_w*S_w + P_o*S_o$), precise enough to be applied in pressure and stress analyses.

3.3. *Stresses redistributions with saturation*

The parameters used in the stress model are listed in Table 2. Corresponding to the changes of rock strength and pore pressure, the effective normal stresses shift significantly away from the wellbore, along with an increase of the shear stress (Fig. 5). This leads to more rock that is more likely to experience shear failure in higher water saturation areas. Then, stresses move back towards the

Table 2. Parameters used in the geomechanical (stress) model

Rock Mechanical Properties					Reservoir Flow Properties					Geometry Parameters		
E (Pa)	ν	σ_h (Pa)	C_o (Pa)	φ	ϕ_i	k_i (m^2)	P_2 (Pa)	μ (Pa/s)	Q (m^3/s)	R_2 (m)	R_1 (m)	h (m)
3×10^9	0.45	28×10^6	0.5×10^6	30°	0.3	0.3×10^{-12}	10×10^6	0.01	1.157×10^{-3}	50	0.1	10

opening because of the increased pressure at later stages of water invasion. The stress increase reaches several MPa in magnitude.

3.4. Propagation of the plastic zone

Both strength reduction and increased stress have significant impacts on rock stability and behavior after water breakthrough. Stability influence is interpreted in terms of a critical radius (R_c) in Fig. 6 that defines the boundary between elastic and plastic zones around a wellbore. The solid lines describe the propagation of R_c with saturation for sands with different initial cohesive shear strengths (C_{o_init}). Dimensionless critical radius is defined as the ratio of R_c to wellbore radius R_1. Clearly, saturation has a large impact on the plastic yield zone: R_c increases rapidly with the increase of saturation.

Even though it is hard to rigorously quantify the effects of chemical reactions, one qualitative way is to consider a reduced initial cohesive shear strength, as shown in Fig. 6. When the rock initial strength is decreased from 0.5 to 0.4 MPa because of the chemical reactions discussed above, the plastic radius increases around 2.5 times at the same saturation (e.g. S_w = 0.45). This indicates that strength-weakening chemical reactions can greatly affect the amount of failed rock around a wellbore.

Compared to the dashed lines that treat rock strength as a constant, i.e. no capillary strength appears and rock stability changes only result from pore pressure variations, the capillary effect is far less significant than the effect of relative permeabilities unless the initial rock strength is relatively low (e.g. C_{o_init} = 0.4 MPa). Considering that the magnitude of capillary strength (on the order of kPa) is much lower than rock strength (on the order of MPa), this defines when capillary strength plays an important role in stabilizing sand: after most of its initial strength has been destroyed due to high shear stress or lost due to chemical reactions. Only at this stage can the effect of capillarity become a significant factor.

Furthermore, after shear failure, the only possible cohesive bond existing among sand particles is capillary tensile strength. Therefore capillarity plays a dominant role in the final phase of erosion and transport of failed sands into the wellbore. Since capillary strength is shown to depend only on water saturation, the sanding rate for each value of saturation becomes constant until either the cohesive strength or the destabilizing forces, e.g. fluid seepage force and loading force resulting from shear stresses, are changed, which leads to so-called episodic sand production after an oil well starts to produce water [5].

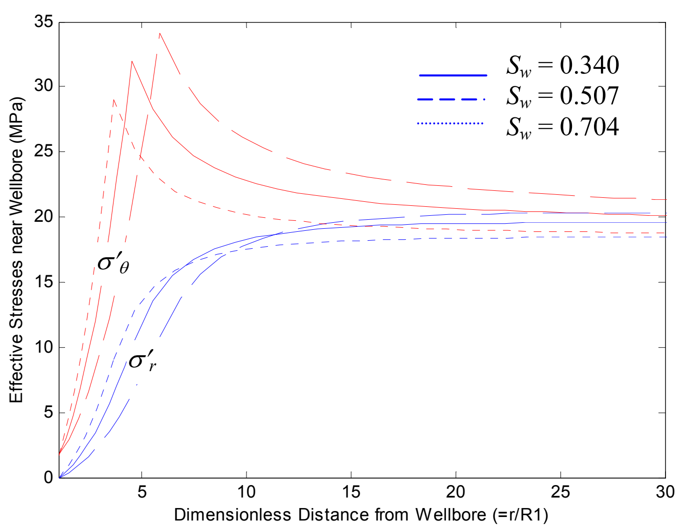

Fig. 5. Variations of effective stresses with saturation

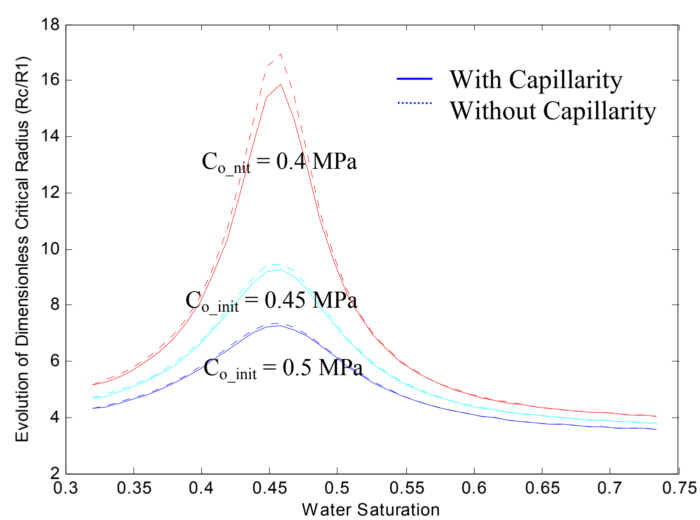

Fig. 6. Effect of capillary strength on plastic yield front

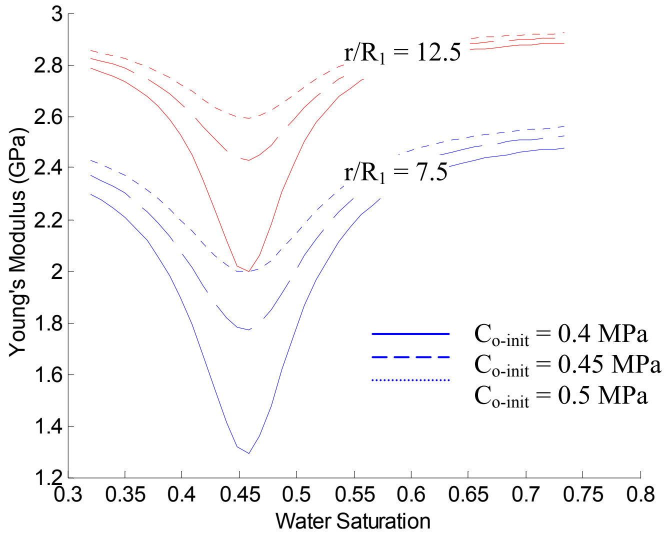

Fig. 7. Young's modulus vs. water saturation

3.5. *Rock softening*

To investigate rock nonlinearities in stressed biphasic environments, both stress variables (σ'_θ and σ'_r) from the stress model and water-related rock strength (C_o) from the strength model serve as inputs to Eqs. (19) and (20).

Corresponding to shear stress redistribution that significantly changes with water breakthrough (Fig. 7), the Young's modulus decreases from 2.3 GPa to 1.3 GPa, a loss of about 45%, before it regains part of stiffness because of pressure recovery and therefore effective stress release. Furthermore, the magnitude of modulus loss and stress increase with water saturation depends on location in the rock and its initial strength: the farther the rock is located from the well (r/R_1 = 7.5, 15) and the stronger it is (0.4, 0.45, 0.5MPa), the less the modulus loss and the stress increase. This confirms experimental observations that weaker rock is more sensitive to changes in moisture content [29].

4. CONCLUSIONS: WHY SAND FAILS AFTER WATER BREAKTHROUGH

Analytical research and model development has generated a new rock strength model to capture the effects of capillarity and chemical reactions, a new fluid pressure model based on micromechanics, and a coupled analytical elastoplastic model for stress estimations around an oil well. These efforts have helped to identify and study sand instability mechanisms so that the question of why sand fails after water intrusion can be more logically approached.

In summary, with an increase in water saturation, sands tend to become weaker (strength reduction) and softer (stiffness reduction), while loading stresses (effective stress and shear stresses) are elevated and the maximum shear stress moves outward into the reservoir, affecting a larger volume of rock. Consequently this rock is more likely to experience shear failure that destroys or damages the cohesive or interlocked fabric. Furthermore, weakened sands are more easily detached from the rock matrix because of the decrease of the tensile capillary strength with an increase in water saturation. Since the capillary strength only depends on water saturation if the rock and fluid properties are fixed, the sanding rate for each saturation value should be constant until the destabilizing forces are changed, which leads to the observed episodic sand production that develops after water breakthrough.

ACKNOWLEDGEMENT

The authors thank Dr. Denis Heliot and Dr. Steve Chang from Schlumberger for having initiated the studies. The technical communications with Dr. Luis C.B. Bianco from PetroBras, Dr. Mike Bruno from Terralog Technologies Inc., and Dr. Euripides Papamichos from Aristotle Univ. of Thessaloniki are deeply appreciated.

NOMENCLATURE AND UNITS

C_o	cohesive strength of the rock, Pa
C_{o_init}	initial cohesive strength, Pa
C_{o_ch}	cohesive strength affected by chemical reactions, Pa
E	Young's modulus, Pa
f_w, f_o	water and oil production fraction, dimensionless
F_c	capillary bond force, N
k	absolute permeability of reservoir, m^2
k_{rw}, k_{ro}	water and oil relative permeabilities, m^2
m_E, n_E	coefficients for modulus nonlinearity, dimensionless
ΔP	capillary pressure, Pa
P_w, P_o	water and oil pressures, Pa
P_2	far-field reservoir pressure, Pa
Q	fluid production, m^3/s
Q_w, Q_o	water and oil production rates, m^3/s
r	radius of liquid bridge between particles, m distance from wellbore, m
R	radius of the particles, m
S_w	water saturation, dimensionless
S_{wc}	connate water saturation, dimensionless
S_{oi}	immobile oil saturation, dimensionless
S_{w0}	the saturation at which capillary pressure becomes zero, dimensionless

α	volume angle of wetting fluid, radian
β	failure angle ($= \pi/4 + \varphi/2$), radian
γ	surface tension between two fluids, N/m
φ	internal friction angle defined in Mohr-Coulomb, degree
ϕ	rock porosity, dimensionless
η	the coefficient defined to balance porosity difference between the model and reality, dimensionless
σ'_r, σ'_θ	effective radial and tangential stresses, Pa
σ_{T_C}	capillary tensile strength of the rock, Pa
σ_{UCS}	Uniaxial Compressive Strength, Pa
μ_o, μ_w	oil and water viscosity, Pa·s
ν	Poisson's ratio, dimensionless

REFERENCES

1. Bailey, B., M. Crabtree, J. Tyrie, F. Kuchuk, C. Romano, and L. Roodhart. 2000 Spring. Water Control. *Oil Field Review*: 30-50.
2. Skjærstein A., J. Tronvoll, F.J. Santarelli, and H. Jøranson. 1997. Effect of water breakthrough on sand production: experimental and field evidence. SPE 38806, *the SPE Annual Technical Conference and Exhibition, San Antonio, TX, USA, October 1997.*
3. Vaziri, H., B. Barree, Y. Xiao, I. Palmer, and M. Kutas. 2002. What is the magic of water in producing sand? SPE 77683, *the SPE Annual Technical Conference and Exhibition, San Antonio, TX, USA, October 2002.*
4. Hall, C.D., and W.H. Harrisberger. July 1970. Stability of sand arches: a key to sand control. *J. Pet. Tech.*: 821-829.
5. Bruno, M.S., C.A. Bovberg, and R.F. Meyer. 1996. Some influences of saturation and fluid flow on sand production: laboratory and discrete element model investigations. SPE 36534, *the SPE Annual Technical Conference and Exhibition, Denver, Colorado, USA.*
6. Bianco, L.C.B., and P.M. Halleck, 2001. Mechanisms of arch instability and sand production in two-phase saturated poorly consolidated sandstones. SPE 68932, *the SPE European Formation Damage conference, Hague, Netherlands, May 2001.*
7. Colback, P.S.B. and B.L. Wild. The influence of moisture content on the compressive strength of rocks. In *Proceedings of 3rd Canadian Symposium of Rock Mechanics, 65-83, 1965.*
8. Forsans, T.M., and L. Schmitt. 1994. Capillary force: the neglected factor in shale stability", In *Proc. Eurock'94, 71-84, Delft, 1994.*
9. Papmichos, E., M. Brignoli, and F.J. Santarelli. 1997. An experimental and theoretical study of a partially saturated collapsed rock. *Mechanics of Cohesive-Frictional Materials* 2: 251-278.
10. Gutierrez, M., L.E. Øino, and K. Høeg. 2000. The effect of fluid content on the mechanical behaviour of fractures in chalk. *Rock Mechanics and Rock Engineering* 33 (2): 93-117.
11. Brignoli, M., F.J. Santarelli, and C. Righetti. Capillary phenomena in an impure chalk. In *Proceedings of Eurock '94, 837-843, Balkema, Rotterdam, 1994.*
12. Hawkins, A.B. and B.J. McConnell. 1992. Sensitivity of sandstone strength and deformability to changes in moisture content. *Quarterly Journal of Engineering Geology* 25: 115-130.
13. Dyke, C.G. and L. Dobereiner. 1991. Evaluating the strength and deformability of sandstones. *Quarterly Journal of Engineering Geology* 24: 123-134.
14. Dube, A.K. and B. Singh. January 1972. Effect of humidity on tensile strength of sandstone. *J. Mines, Metals and Fuels* 20(1): 8-10.
15. Boretti-Onyszkiewicz, W. 1966. Joints in the Flysch sandstones on the ground of strength examinations. In *Proc. 1st Cong. Int. Soc. Rock Mech., 1, 153-157, Lisbon.*
16. Han, G. and M.B. Dusseault. 2002. Quantitative analysis of mechanisms for water-related sand production. SPE74747, In *Proceedings of the SPE International Symposium and Exhibition on Formation Damage Control, Lafayette, LA, USA. February 2002.*
17. Han, G. and M.B. Dusseault. 2002. Strength variations with deformation in unconsolidated rock after water breakthrough. Paper#2002-22, In *Proceedings of the 2002 International Symposium of the Society of Core Analysts, Monterey, CA, USA, September 2002.*
18. Han, G., M.B. Dusseault, and J. Cook. 2002. Quantifying the behaviors of rock capillary strength in unconsolidated sand. SPE78710, *the SPE/ISRM OilRock Conference, Irving, TX, USA, October 2002*.
19. Han, G. and M.B. Dusseault. 2003. Rock stress analysis with a simplified capillarity model. In *Proceedings of EURO-Conference on Rock Physics and Geomechanics: Micromechanics, Flow and Chemical Reactions, Kijkduin, The Netherlands, 7-11 September 2003.*
20. Lord, C.J., C.L. Johlman, and D.W. Rhett. July 1998. Is capillary suction a viable cohesive mechanism in chalk? SPE 47310, *the SPE/ISRM Eurock '98, Trondheim, Norway.*
21. Schubert, H. 1984. Capillary forces – modelling and application in particulate technology. *Powder Tech.* 47: 105-116.
22. Gregory, A.R. 1976. Fluid saturation effects on dynamic elastic properties of sedimentary rocks. *Geophysics* 41(5): 895-921.
23. Hadizadeh, J. and R.D. Law, 1991. Water-weakening of sandstone and quartzite deformed at various stress and strain rates. *Int. J. Rock Mech. Min. Sci. & Geomech. Abstr.* 28(5): 431-439.
24. Rao K.S. G.V. Rao, T. Ramamurthy. 1987. Strength of sandstones in saturated and partially saturated conditions. *Geotechnical Engineering* 18(1): 99-127.

25. Duncan J.M. and C. Chang. 1970. Nonlinear analysis of stress and strain in soils. *Journal of the Soil Mechanics and Foundations Division. In Proceedings of the American Society of Civil Engineers, SM5: 1629-1652, September 1970.*

26. Kulhawy F.H. 1975. Stress deformation properties of rock and rock discontinuities. *Eng. Geol.* 9: 327-350.

27. Santarelli, F.J., E.T. Brown, and V. Maury. 1986. Analysis of borehole stresses using pressure-dependent linear elasticity. *Int. J. Rock Mech. Min. Sci. & Geomech. Abstr.* 23(6): 445-449.

28. Tronvoll J. 1993. *Investigation of cavity failures for sand production prediction.* PhD Thesis, Norwegian Technical University, Trondheim, Norway, 20-48.

29. Dyke C.G., L. Dobereiner. 1991. Evaluating the strength and deformability of sandstones. *Quart. J. Eng. Geol.* 24: 123-134.